MICHIGAN STATE UNIVERSITY

CYCLOTRON LABORATORY

SUPERCONDUCTING CYCLOTRONS

FOR

NEUTRON THERAPY

H.G. BLOSSER

AUGUST 1988

MSUCP-52

TABLE OF CONTENTS

energy.) The (d,Be) reaction has an intensity or targetry advantage due to the fact that the yield of neutrons from this reaction is ten times higher than the yield from the proton reaction, or for a given neutron dose rate, the deuteron beam can have 1/10th the current required with a proton beam. Even though proton and deuteron results are considered clinically indistinguishable on an overall basis, there is evidence that the low energy tail of the proton spectrum is disadvantageous with respect to skin sparing and proton facilities then frequently use less than a full stopping thickness target to reduce the low energy tail thereby still further increasing the beam current required.

In the case of the superconducting cyclotron neutron therapy facility, the choice of projectile is much more open than in the case of the room temperature cyclotron -- the rule a given cyclotron magnet will bend protons of twice the energy still holds but the size of the cyclotron is a much less dominating issue since the cyclotron is small for either protons or deuterons. Other significant factors can then be brought into consideration, the two of these which are most important being the need to easily provide good axial focussing for the beam and the advantages which go with setting the operating frequency of the acceleration system at a value where commercial rf power equipment is broadly available.

The need to provide good axial focussing is inherently more demanding in a superconducting cyclotron than in a room temperature cyclotron because the solenoidal coil which is used to produce the high field does not add to the strength of the azimuthally varying components of the field which are the components producing the axial focussing. These components come into the focussing strength in a fractional way versus the main field strength; the designer must then adapt to a situation in which the forces which provide the axial focussing are, in a relative sense, much weaker than they would appear to be in a room temperature cyclotron. Superconducting cyclotrons then adopt the dee-in-valley design first introduced in the 50 MeV cyclotron at the University of California at Los Angeles[2] and particularly perfected in the series of cyclotrons built by the AEG Company of Germany the first of these being the 50 MeV deuteron cyclotron at Karlsruhe[3]. With this dee-in-valley design the magnet gap in the hill region needs only to provide space for the beam and much stronger focussing results. In cyclotrons (except 2nd stage booster cyclotrons), a weak point in the focussing occurs near the center and a 3-sector design is therefore helpful in that the focussing forces "come on" at a smaller radius than in a 4-sector design. Pending detailed evaluation of the focussing, it is reasonable to consider either three or four sectors as possible alternates, but with a strong plus in favor of the 3-sector system, where solutions which provide adequate focusing have already been demonstrated and where the inherently greater focussing strength is in any case always an advantage.

The choice of rf frequency is a centrally important design decision in any cyclotron, the rf system being invariably the point where the largest number of puzzling or unexpected phenomena occur. A neutron producing cyclotron, since it operates at only one energy needs an amplifier which runs at only one frequency and this is a great simplification relative to the rf complexity of a variable energy cyclotron. For superconducting cyclotrons, the rf frequency needed is typically much higher than in room temperature cyclotrons since the frequency goes up in proportion to the magnetic field and

yoke would be thinner by approximately 30% which would lighten the cyclotron magnet by nearly that fraction down to perhaps 18 tons but the rf frequency of 146 MhZ is again an awkward value with equipment much less available than in the standard fm band.

Another option, Proton C, would be to lower the magnetic field still further to 2.4 tesla which would put the rf frequency at 110 Mhz or just within the standard fm transmitter range. The target radius would increase to 40.8 cm and orbit spacing would be 30% larger and therefore more comfortable than in the deuteron machine. The total weight of the magnet would return to about the same value as the deuteron case but with a slightly larger radius and a somewhat thinner outer wall, which would reduce its effectiveness as a radiation shield. Another moderate difficulty would be less accurate magnet calculations due to the shift of field strength to near the saturation value.

Still another design option, Proton D, would use 4-sectors and four dees operating on the fourth harmonic and an rf frequency of 110 MhZ. This would push the magnetic field still further down to 1.8 tesla, increase the weight of the cyclotron, and generally give no advantage relative to Proton C. A possible alteration of Proton D would be to shift to second harmonic operation which would shift the magnetic field to 3.6 tesla with target radius of 27.3 cm. This would give a quite attractive magnet but the central region would be extremely complicated -- if the acceleration system is to be driven from one amplifier, opposite pairs of dees would need to be coupled and driven in Push-pull mode, an operating regime which has been very troublesome in the Chalk River superconducting cyclotron[4]. The central region design of the Chalk River cyclotron is moreover not compatible with an ion source (the Chalk River cyclotron being intended as a booster for their MP tandem). It is certainly extremely difficult to think of a dee coupling arrangement which would be compatible with an ion source but, if this problem was solved, the magnetic field would increase to a quite desirable range; the intricacies of the central region coupling problem are however indeed formidable.

Reviewing these options we see that Proton C is reasonably comparable to the Deuteron H design -- it however has no very strong advantage relative to that design and has a clear disadvantage in target design since the proton target must be able to withstand ten times the beam current that the deuteron target would need to handle. Even if one were convinced that the unusual proton frequencies required in Proton A and Proton B were insignificant problems the target power problem would remain for these designs as well and the gain in magnet weight in these options is not large. Considering all these factors it then continues to appear that the 3-sector, third harmonic, 50 MeV deuteron design selected for Harper Hospital remains the design of choice for a superconducting neutron therapy cyclotron.

III. Engineering Features of the Harper Hospital Cyclotron

In September of 1984 the National Superconducting Cyclotron Laboratory of Michigan State University began a joint project with Harper-Grace Hospitals Inc. of Detroit, Michigan for the purpose of designing and constructing a neutron therapy facility based on a superconducting cyclotron. After testing of the cyclotron at Michigan State, the unit is to be installed in the

A. The Superconducting Coil for the Harper Hospital Cyclotron

As indicated in the previous section, the superconducting coil for the medical cyclotron is basically a split solenoid with a full diameter warm bore; several room temperature penetrations also pass through the coil at the solenoid split, as for example the target shaft at the right side of Figure 6. The helium cooling system must allow the coil to rotate through a full 360° about an axis perpendicular to the axis of the solenoid, and must provide a reasonable helium reserve since some users will prefer to fill the coil by batch transfer from dewars of purchased helium[5]. The coil is also exposed to a significant amount of neutron heating when the cyclotron is in operation (approximately 0.3 watts) and this heat load is strongly localized on the side of the coil near the neutron production target. The neutron flux hitting the coil is reduced by a set of one inch thick tungsten blocks mounted on the room temperature wall of the cryostat in the vicinity of the neutron production target -- these blocks show in Figure 5 at the lower right of the center point.

The magnetic field in the cyclotron is 4.6 tesla at the center corresponding to an accelerating system frequency of 105 MHz to match the orbital frequency of deuterons in third harmonic mode. Away from the magnet center the field is segmented into strong focussing hills and valleys, the peak field on the hills reaching 5.54 tesla. In the superconducting coil the peak field is 4.9 tesla.

An important design attribute of the coil and cryostat is compactness; the bulk of the weight of the cyclotron is in the portion of the iron yoke which passes around the outside of the coil and cryostat; minimizing the cross-sectional area of the coil-cryostat assembly has a large effect in reducing the weight of the yoke, the weight of the counterweight, and the structural requirements on the main support ring assembly. These factors argue for a high current density in the winding and a small helium storage volume. The small helium storage volume opposes another desired attribute, namely to extend the period between helium fills, and the high current density must balance against the increased probability of premature quenches. The overall coil heat leak is an additional obviously important factor affecting these design compromises, lower heat leak allowing either extended filling intervals or smaller helium storage volumes.

The design solution which has been adopted for the Harper cyclotron uses a 13,000 amp/cm^2, epoxy impregnated, intrinsically stable winding. Figure 7 is a photograph of a cross-sectional cut through a test winding sample, the sample being approximately three-quarters of the length and one-quarter of the radial build of one of the real split solenoid halves. The conductor is rectangular, 0.034 inch by 0.054 inch with 0.001 to 0.002 inch of Formvar insulation, and is wound in a carefully ordered array with layer to layer insulation consisting of "Stycast" impregnated wrapping paper. At each end of each layer, a G-10 wedge is inserted corresponding to a full 360° ramp; the winding is therefore on every turn a true helix. The wedge system removes the need for the wire width to be some even sub-multiple of the coil cavity dimension since each layer can be wound to the point where it fills the coil pocket down to the point where the remaining area just matches the area of the

the end of the underlying layer and the turn at the beginning of the overlying layer.

Figure 9 is a photo of the coil as the final layer was being wound and before installation of the outer G-10 insulation. An additional feature of the median plane bridge which shows in the photo but not in the section view of Figure 8, is the array of stainless steel spacer plates which separate the G-10 end plates of the coil cavities. The possibility of excessive stress concentrations at the ends of these plates is a factor discussed in the next section in connection with the issue of coil quenches.

The helium venting system for the coil is based on a patented[7] array of tubes one of which is always connected to the high point of the liquid vessel and each of which wraps fully around the coil in a vertical plane so as to have a high point which is above the liquid level in the coil. The lines are also structured so that liquid which enters lines when they are connected to the bottom of the coil will drain back into the coil rather than being passed to the warm exit. Additional details of this system are described in the above reference.

B. Operating Experience with the Harper Cyclotron Magnet

In its first turn on, the superconducting magnet for the Harper cyclotron quenched at an operating current of 95 amps, i.e. at less than half of the design operating current of 203 amps. In the ramp-up, the coil gave off occasional metallic pinging sounds including a loud ping just at the time of the quench. In following ramps the pinging sounds repeated, and a training phenomena was observed with the quench current mostly increasing from one run to the next as indicated in Figure 10. The pinging sounds exhibited a hysteresis effect in that, if the upward ramp was stopped prior to a quench and the magnet was ramped down, the sound did not start immediately on the downward ramp but rather after a lag of approximately 30 amps, after which the coil would ping on the downward ramp in much the same fashion as on the upward ramp.

Careful review of the design features of the coil led to two primary hypotheses as to the cause of the premature quenching. A first hypothesis was stress overload in the median plane bridge separating the two halves of the solenoid. This bridge (which shows in Figure 9) consists of radial stainless steel ribs 0.25 inch thick by 2.8 inches high by 2 inches wide, spaced on approximately 2 inch centers around the coil; these spacers separate the G-10 coil end plates which are 0.5 inches thick. The average axial force on the median plane bridge was calculated to be 1300 psi -- taking the fractional area of the stainless ribs into account gives a load of 8,700 psi in the ribs -- stress concentrations at the somewhat complicated joint between the ribs and the G-10 might give still higher stresses which could lead to localized fractures of the G-10 laminate. This hypothesis fails to provide a ready explanation of the ramping-down sounds and so detailed calculations of stress concentrations were not made.

The second hypothesis, and the one which appears to be confirmed by later results, was that the coil was sliding axially on the bore tube due to inadequate bonding between the bore tube and the coil; as the magnetic force

the upper training curve in Figure 10; the coil has thereafter operated as needed.

Post-mortem analysis of the coil stress calculations uncovered a significant error which is thought to be the cause of the original quench difficulty. The error came in assuming that the 0.001 inch layer of Formvar insulation had the same elastic properties as the Stycast epoxy. In fact the modulous of the Formvar is about 100,000 psi, i.e. the Formvar is a very rubbery, springy material and even though it appears as a very thin layer, it has a dominating effect on the effective elastic modulous of the overall coil[8]. Stress calculations with the Formvar correctly included showed a lift-off condition consistent with the observed quench behavior. With this result in hand, the design solution to avoid this difficulty in future coils is straight-forward, namely to increase the radial preload in the coil by about 30%; this can be accomplished by either increasing the winding tension or by adding a small layer of aluminum banding to the outside of the coil. Detailed consideration as to the ease with which each of these options can be implemented will determine which to use.

C. Magnetic Field Characteristics

Pillbox type superconducting cyclotron magnets are designed using 2-dimensional cylindrical relaxation calculations in which the iron density in any r-z segment is taken as the azimuthal average of the iron density in the corresponding r-z segment of the actual 3-dimensional magnet. In experimental comparisons, such 2-dimensional calculations give values which agree with the azimuthal average of the experimentally measured magnetic field to an accuracy of typically one part in 200[9].

The precision with which this azimuthal average of the magnetic field must be fixed in the actual cyclotron is much higher than the 1 in 200 which the design calculations are able to achieve. This is due to the fact that this "average field" is the quantity which largely determines the orbital frequency of the particles -- in an isochronous cyclotron this frequency must accurately match the accelerating electrode frequency or else the particles will slip out of phase with the accelerating voltage and be deaccelerated as a consequence of the absence of phase stability in an isochronous system. In addition, for simplicity, the superconducting medical cyclotron (in contrast with other superconducting cyclotrons) is designed with only one electrical winding in the magnet so that the spatial distribution of ampere-turns is not available as am empirical adjustment to use in matching the isochronism requirement of the cyclotron. The effect of a specific average field error depends on the spatial extent of the error, i.e. on the number of orbits impacted by the error -- for an error effecting all of the cyclotron orbits the magnet tolerance to satisfy a ±20° rf phase tolerance is ±1 part in 12,000. Errors which effect a subset of the orbits may have larger magnitude in inverse proportion to the fraction of the total number of orbits effected by the error.

Since the required average field accuracy is much tighter than design calculations are able to achieve, a design concept based on mapping of the magnetic field and machining corrections into the iron pole tip must be used. Fortunately the 1 in 200 accuracy of the advance calculations is sufficient to

displacement example results in a positive ridge along the leading edge of the displaced pole tip, a negative ridge along the lagging edge of the displaced pole tip, and reverse sign ridges of half strength at the leading and lagging edges of the other two pole tips. Working with such intuitive signature concepts, error contour maps are interpreted in terms of probable magnet geometry errors and corrections are introduced to compensate for these errors. The result of this process for the Harper Hospital magnet was a magnet which was free of errors to a considerably greater degree than was actually required to have well behaved orbits -- this additional degree of field symmetry is useful in reducing the sensitivity of the beam to shifts in operating parameters, the sensitivity to the exact value of the accelerating voltage being the most important of these effects.

D. Acceleration System and Ion Source

After the magnetic field mapping, installation of the accelerating electrodes began and at the time of writing of this paper (August 1988) was at the point of being nearly complete. Figure 15 shows a photo of one pole of the magnet with the accelerating electrode structure mounted in place. As this pole is raised into the yoke, "dee stems" from the other half of the yoke will come into contact with the cylindrical mounting blocks seen on top of each "dee" in the photo. The third-harmonic rf mode in which the medical cyclotron will operate requires the voltage on all three dees to be electrically in phase; the dees are therefore metallically tied together in the center as can be seen in the figure. Each dee has two coaxial stems running up and down from the dee proper, as can be seen in Figure 6. The electrical structure of the resonator is consequently equivalent to six capacitively-loaded, quarter-wave shorted lines with the unshorted end of all the lines connected together. This resonator is driven by a 105 MHz rf amplifier with 25 kw output, this amplifier being a standard unit manufactured by Continental Electronics and normally intended for use as an fm radio station transmitter. The rf drive is coupled to the resonator through an inductive loop in one of the six dee stems; another stem contains pickup loops for amplitude control and for tuning adjustment.

The detailed design of the ion source and central region electrodes for the medical cyclotron is illustrated in Fig. 16 which is a median plane section view showing the source, the portions of the central electrode which penetrate the median plane, and the grounded field shaping electrodes mounted on the tips of the magnet poles. Voltage equipotentials and a typical orbit corresponding to the design central ray of the beam are superimposed on the electrode drawing. Central region orbits are calculated using electric fields computed by a three-dimensional relaxation program; these together with the measured magnetic field information give the Lorentz force needed for the computations. Figure 17 shows the axial motion associated with the trajectory of Figure 16 for two linearly independent solutions; some amplitude growth occurs associated with an overfocussing at an early gap but this is compatible with the aperture and should not adversely effect cyclotron operation.

The absolute size of the orbit pattern in Figure 16 depends on the dee voltage -- for the computations shown in the two figures a peak voltage on the dees of 38 kV relative to ground was assumed. The rf testing program will establish the actual dee voltage which can be produced by the 25 kw transmitter -- when this voltage is known, the central region electrode design

penetrations to pump the beam chamber to the required operating pressure of 1 x 10^{-5} torr. The turbo pump is mounted with its axis of rotation parallel to the rotation axis of the gantry so that gyroscopic effects do not come into play as the gantry rotates and the pump is an invertible design so the operation is independent of the angular setting of the cyclotron gantry. The foreline from the turbo pump feeds off of the gantry through the cyclotron utility arm to one of two mechanical pumps (Leybold-Heraeus TriVac Model D16A) located in the adjacent utility room.

The second mechanical pump is connected to a roughing manifold for backing the cryostat diffusion pump when it is in use, pumping the vacuum locks on the source and target when either of these is being inserted, and, if needed, for pumping on a guard vacuum system on the main pole tip seal, so that if a leak develops in this seal repair can be deferred to the next following annual maintenance period.

G. Control System

Control of the cyclotron uses a Macintosh Plus computer interfacing with the various items of equipment via an Acro 900 interface unit. The operator uses a computer screen, keyboard, and mouse to initiate actions, make settings and observe measurements of status conditions. Figure 21 is a block diagram showing the equipment items involved in the control system and their interrelationships. Figure 22 shows the control screen layout for routine operation of the cyclotron. Shifting to a different control screen is accomplished by clicking the mouse on one of the menu words listed across the top line of the screen; selection of any of these categories will bring up a list of the screens available in that category and clicking on the particular name will bring up the desired screen. Figures 23, 24, and 25 show three such screens which would be brought up to turn on the magnet, the ion source, and the rf system respectively or to check the detailed status of any of those subsystems. On each page the section above the time and name bar is identical and consists of status labels and control buttons for the four major control subsystems. If the control system is in automatic mode, turn on consists of clicking on each of these buttons whenever the label "Standby" shows as the system status; for the "magnet" button this click will change the label first to "Ramping" and then, when the magnet is at operating field, to "Ready" (for use). A dark border around any of the labels indicates that the system is in the "on" state, and clicking will turn the system off. The normal automatic turn-on system uses only these four major buttons. In the upper left of the screen section below the time and label bar, the choice of automatic or manual mode is available -- clicking on the one not darkened will move the system to that mode. The manual mode is for maintenance use -- turning on the magnet in this mode would additionally require clicking on the "Magnet Power" button and clicking on the "Coil Current" label and typing the desired value on the keyboard or alternatively holding on the "up" button below the "Coil Current" label until the current reaches the desired level. Other features of the control system flow in an analogous fashion to these examples. A fully documented manual introduces the user to details of the system.

Other control system features not illustrated here assist the user with identifying the source of an interlock, if an interlock occurs, and with checking or resetting calibration constants in the event such adjustments are

IV. Proton Therapy Systems

For completeness, it seems appropriate for this report to include a brief comment as to the possible future development of related superconducting systems for proton therapy. Proton beams are of interest because they provide an improved alternate to photon therapy in the aspect of allowing a much higher fraction of the total administered dose to be put into the tumor volume, with surrounding normal tissues then receiving a correspondingly reduced dose. This much improved dose localization comes from the physical fact that protons of given energy have a definite range in tissue with a strong maximum in the dose deposited just prior to the stopping point -- the so-called "Bragg peak". Comparing this peak-at-the-stopping-point characteristic with the exponentially falling dose-vs-depth characteristic of photons (or neutrons), it is clear that with the penetration depth of the Bragg peak appropriately adjusted, one can provide a tumor dose which is very highly localized relative to a photon induced dose distribution. Like photons, protons lack the biological advantage of neutrons and neutrons and protons then offer complementary improvements to existing photon therapy, neutrons providing a biological gain and protons providing a treatment localization gain. (Beams of heavier charged ions such as neon combine the advantages of neutrons and protons but the accelerators required to drive such ions deep into the body are much more massive and probably too costly to come into wide use.)

In the US, an energy of 250 MeV has been selected as ideal for proton therapy by a group of MD's, physicists, and engineers, the Proton Therapy Cooperative Group, or PTCOG. Since the direct primary beam is used to produce the treatment, the beam current required is much lower than for processes based on secondary beams such as the neutron system. A proton current of a few nano-amperes appears to be adequate if a sweeper in the beam delivery system is used to distribute the beam over the tumor volume, and a current of 20 nanoamperes is adequate if a scattering system is used to spread the beam.

Protons of 250 MeV are difficult to obtain with a high field isochronous cyclotron due to the very large azimuthal field variation required to override the strong relativistic rise in the average field. The beam current capability of an isochronous cyclotron is also far greater than that required for the proton therapy application. A high field synchrocyclotron then appears as the attractive solution for the proton therapy problem, there being no focussing difficulties since the focussing is provided by the "field fall-off" and typical synchrocyclotron currents being well matched to the beam levels required for the proton therapy application. Exploratory studies of proton therapy have in fact been dominantly conducted on room temperature synchrocyclotrons using older machines which have been retired from service as physics research instruments. A high field synchrocyclotron for 250 MeV is still a rather massive accelerator magnet, weighing about 65 tons versus the 25 tons of the Harper Hospital neutron therapy cyclotron. The 65 ton weight is however still compatible with direct gantry mounting and Figure 27 shows a likely layout for such a system. An external beam and beam transport magnets are of course needed since the proton beam needs to finally stop in the tumor. The array of magnets shown in Figure 27 provides an easy energy changing system by use of the degrading wedge just after the cyclotron and the cyclotron is mounted closer to the axis than in the case of the neutron therapy machine so that overall stresses in the rotation system are reduced.

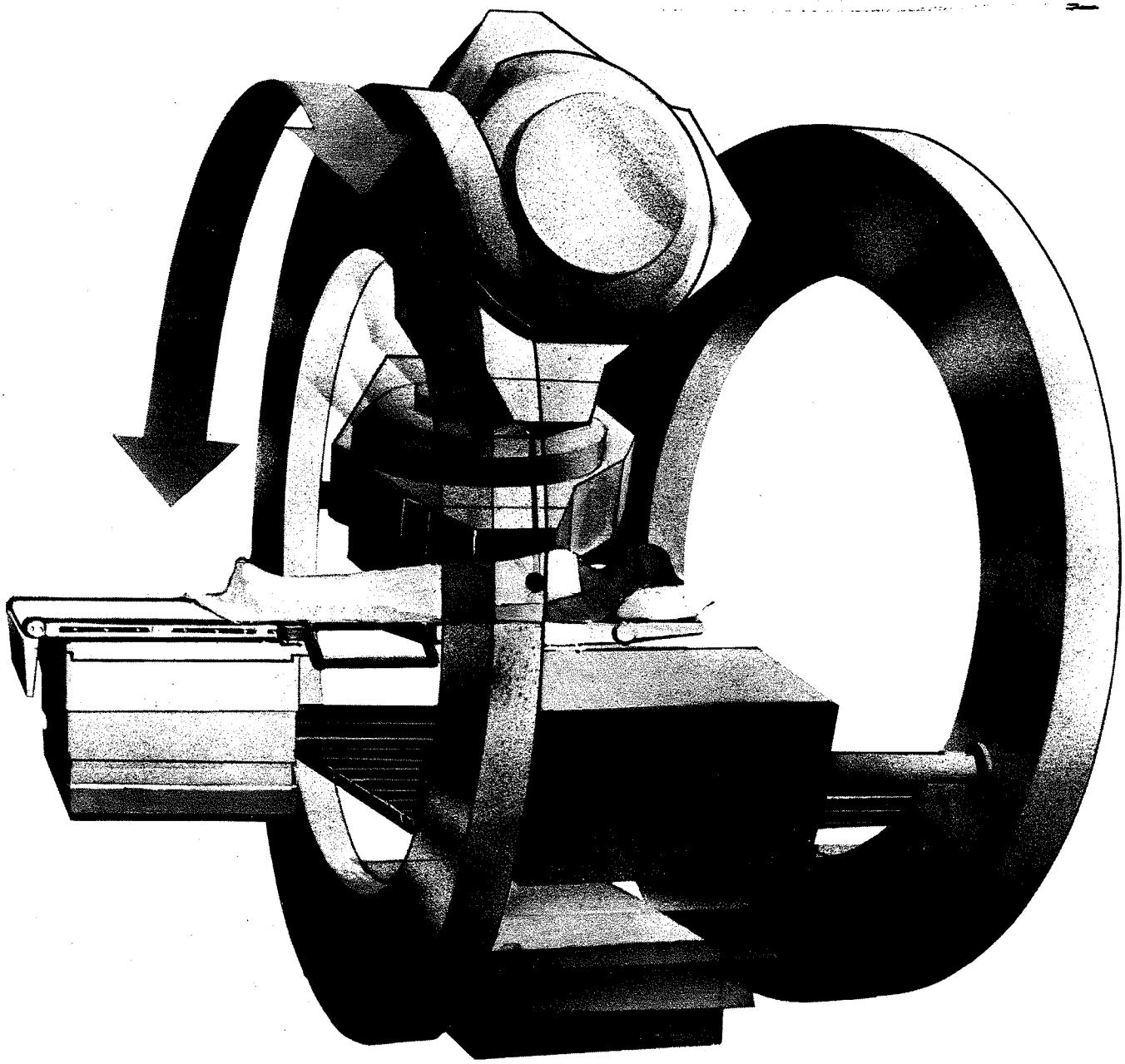

Figure 1. -- Sketch of the "rotating ring" mounting system for the cyclotron. The cyclotron is shown in two positions (above and to the rear of the patient) with the counterweight opposite.

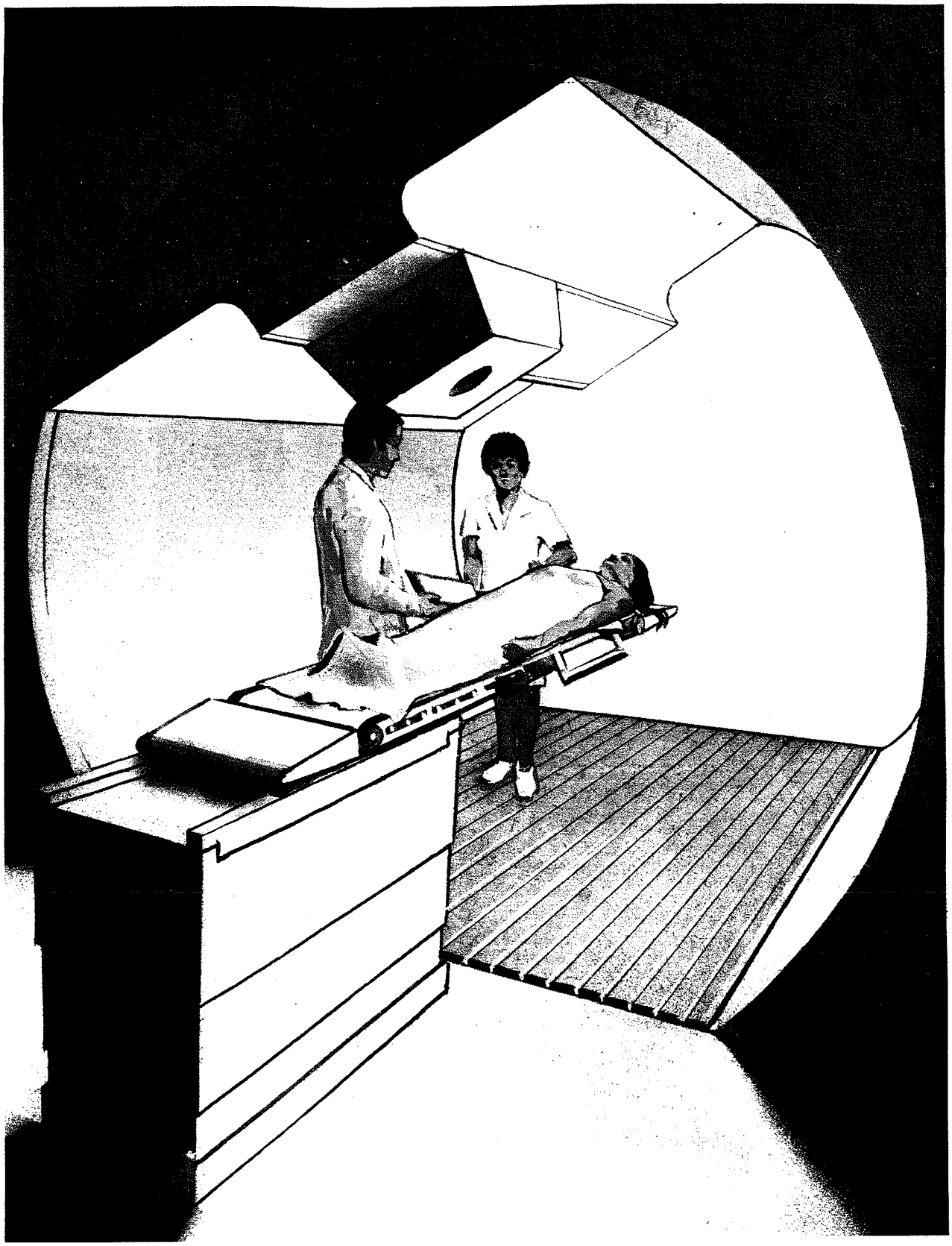

Figure 3. -- Sketch showing the therapy system as it will appear to medical personnel and patients.

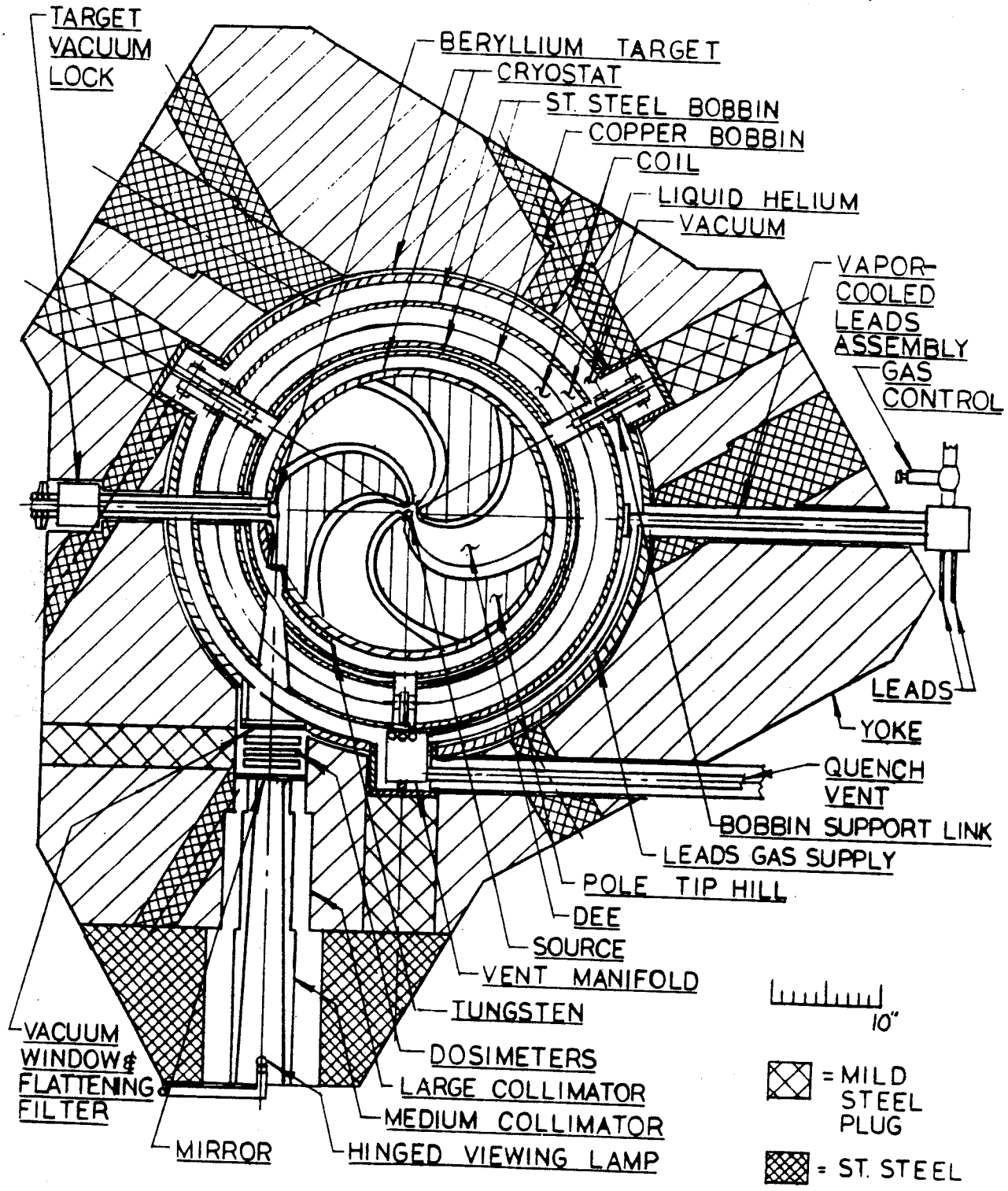

Figure 5. -- Median plane section view of the cyclotron with collimator system at lower left.

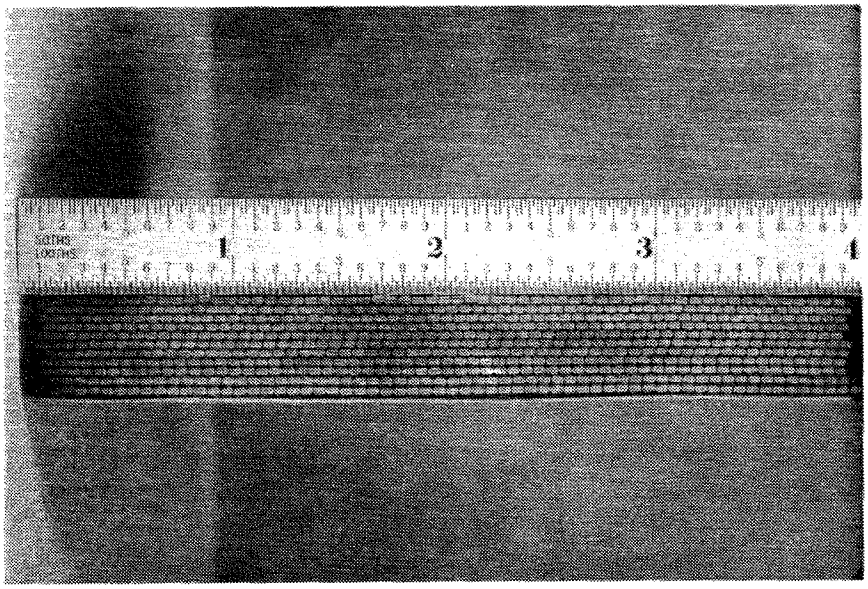

Figure 7. -- Section cut through test winding. The test coil was wound with flattened copper wire of approximately correct size.

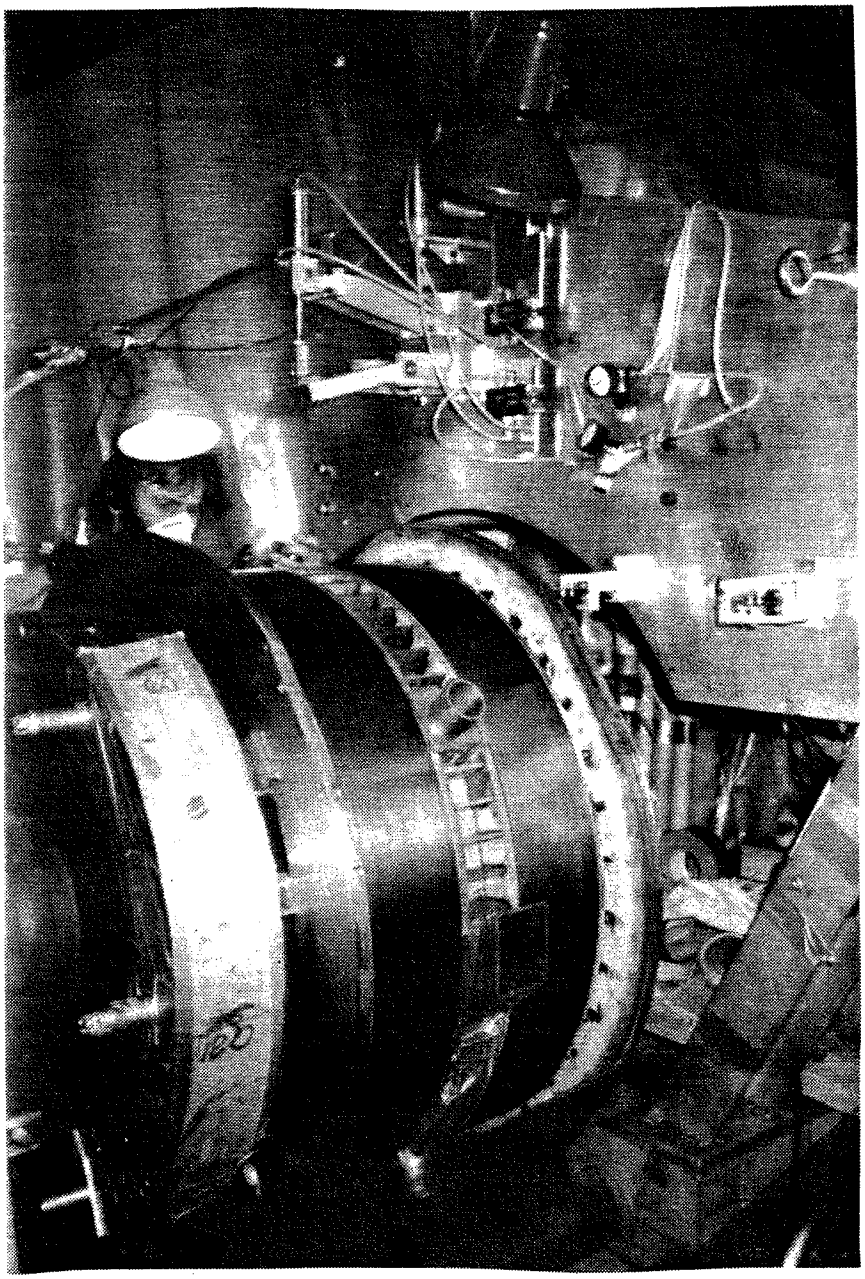

Figure 9. -- Photograph of the main coil on the winding machine. The median plane bridge structure shows between the two coil halves.

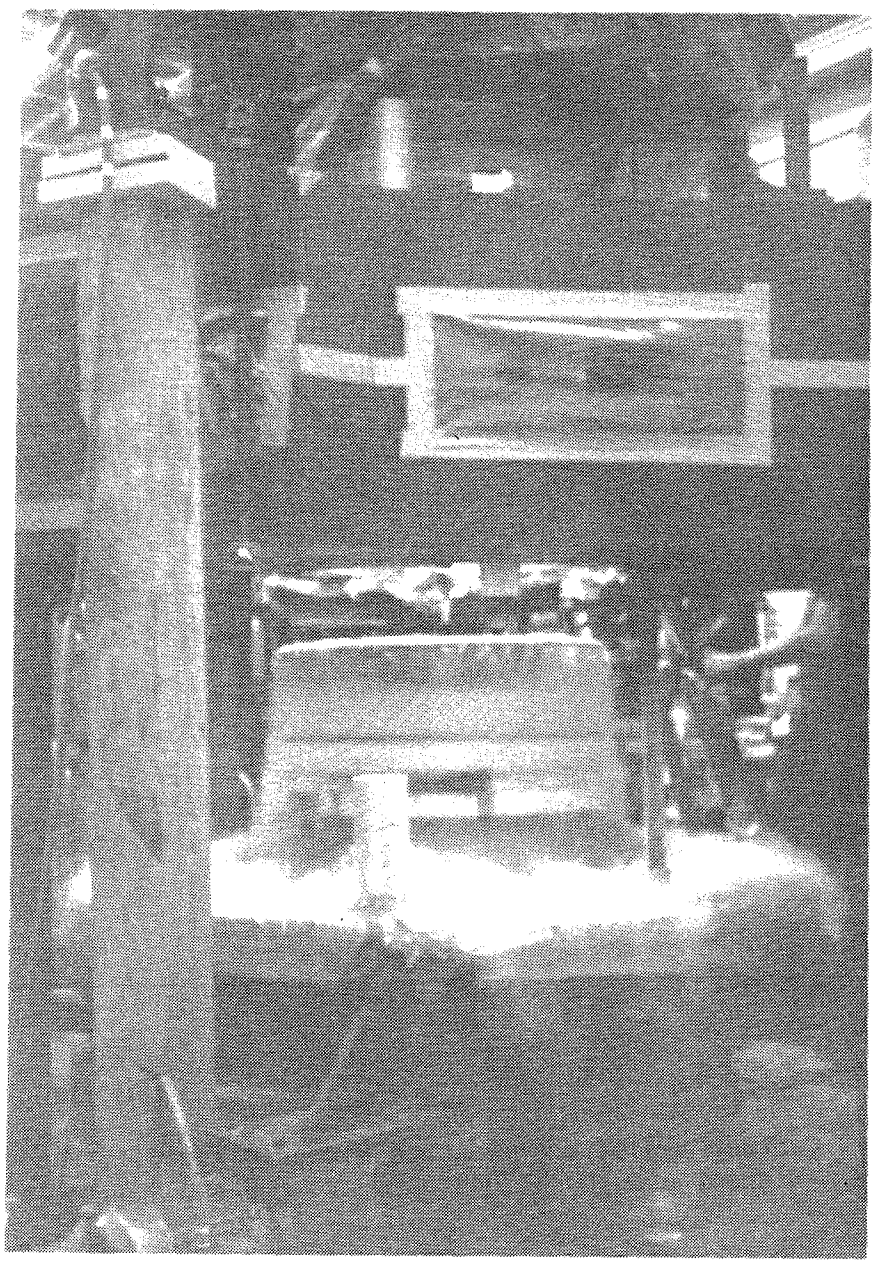

Figure 11. -- Photograph of one of the stretcher rings mounted on the lower magnet pole and filled with liquid nitrogen. (The condensation cloud below the stretcher ring assembly is produced by the nitrogen.)

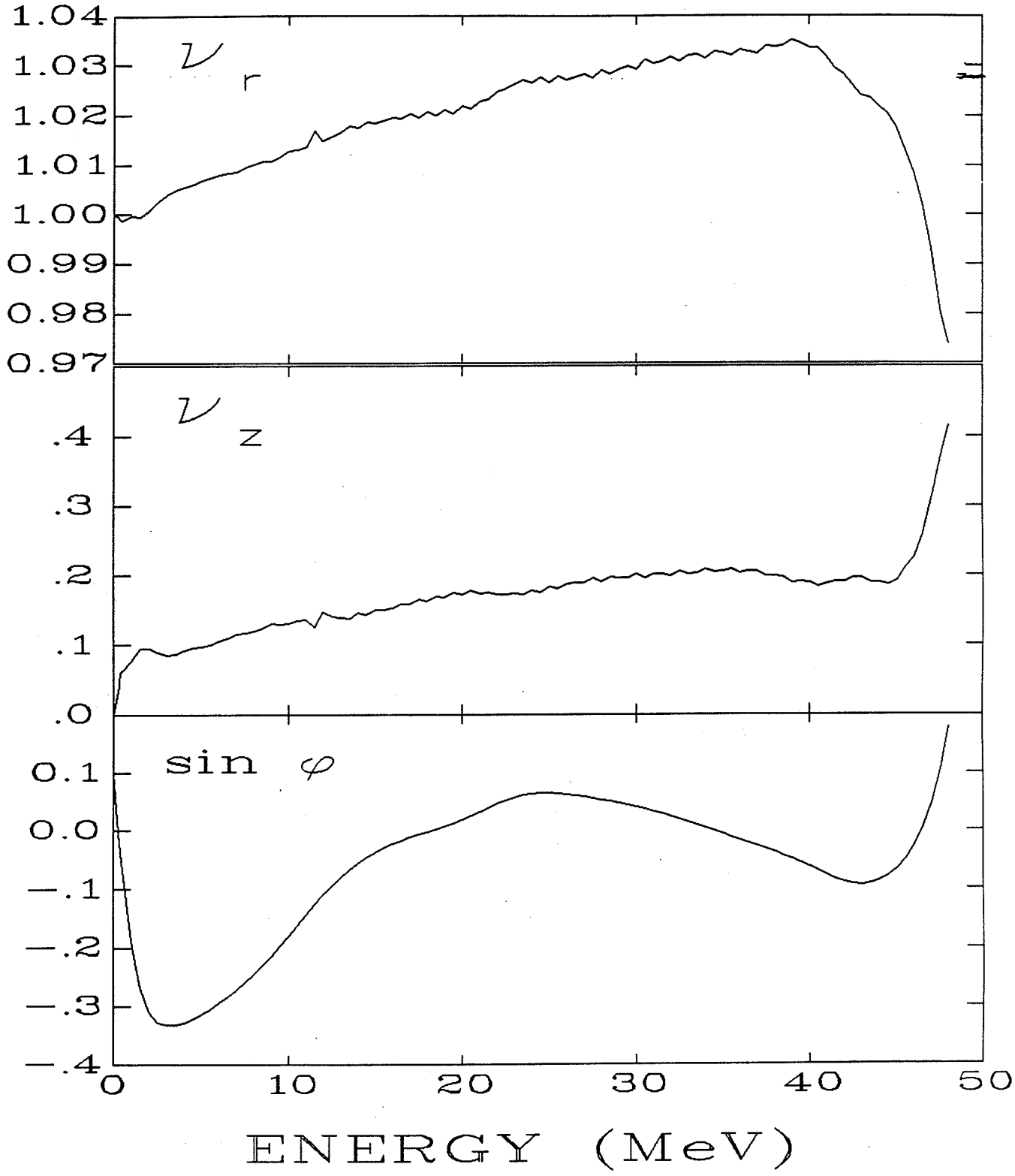

Figure 13. -- Graph of the radial and axial focussing frequencies and the orbital phase of the particle relative to the rf voltage.

Figure 15. -- Photo showing the accelerating electrode structure mounted on the lower magnet pole. The inter-connection of the electrodes shows at the center.

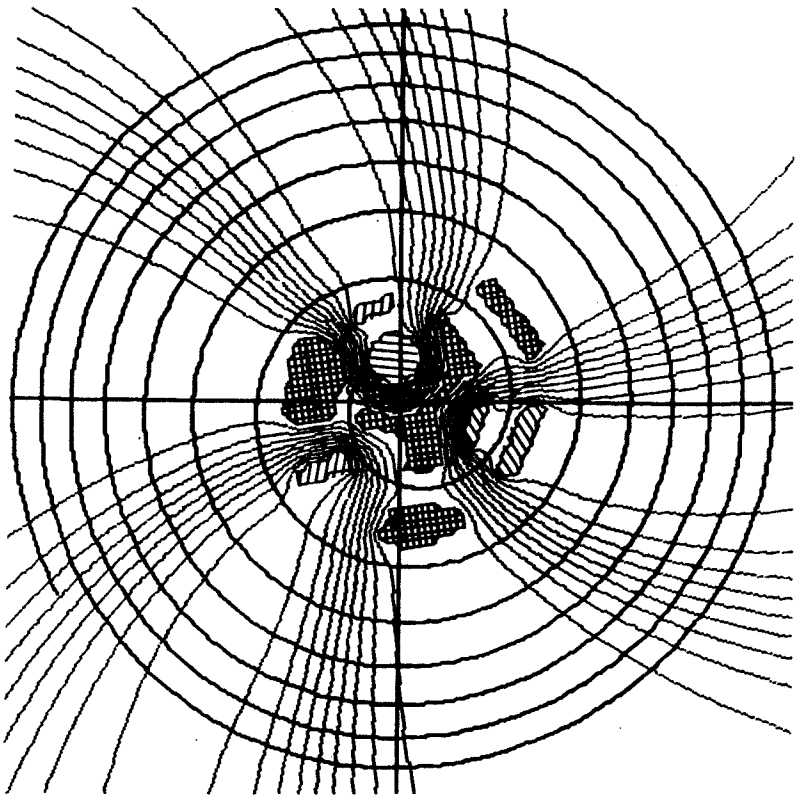

Figure 16. -- Plot of "central ray" orbit superimposed on drawing of the central electrodes including voltage equipotentials produced by the electrodes. Crosshatched electrodes are at the dee potential, electrodes marked with slanted shading are at ground.

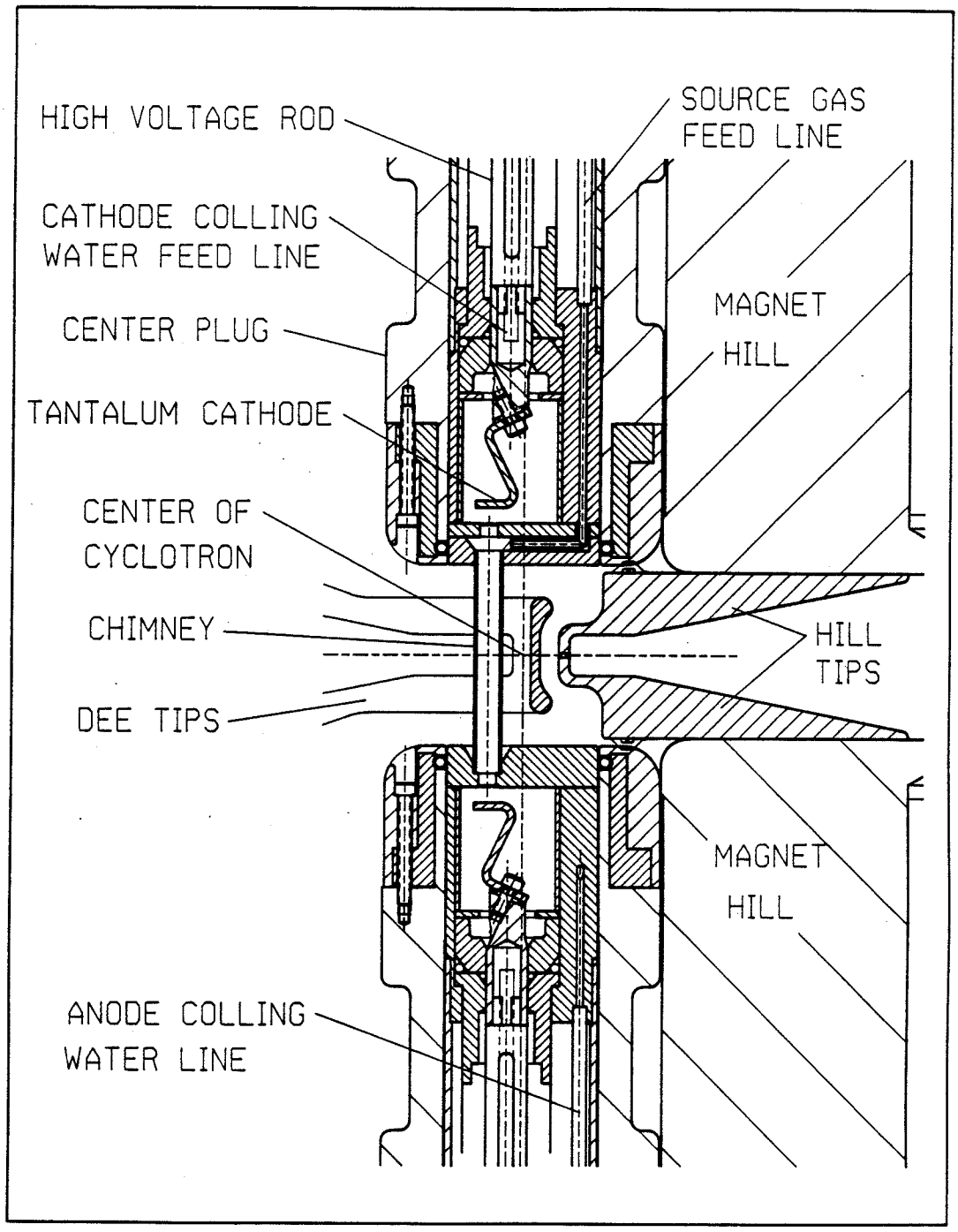

Figure 18. -- Mechanical drawing of the ion source showing cathode assemblies inserted from top and bottom and the thin walled tantalum chimney penetrating through the median plane adjacent to the dee tip.

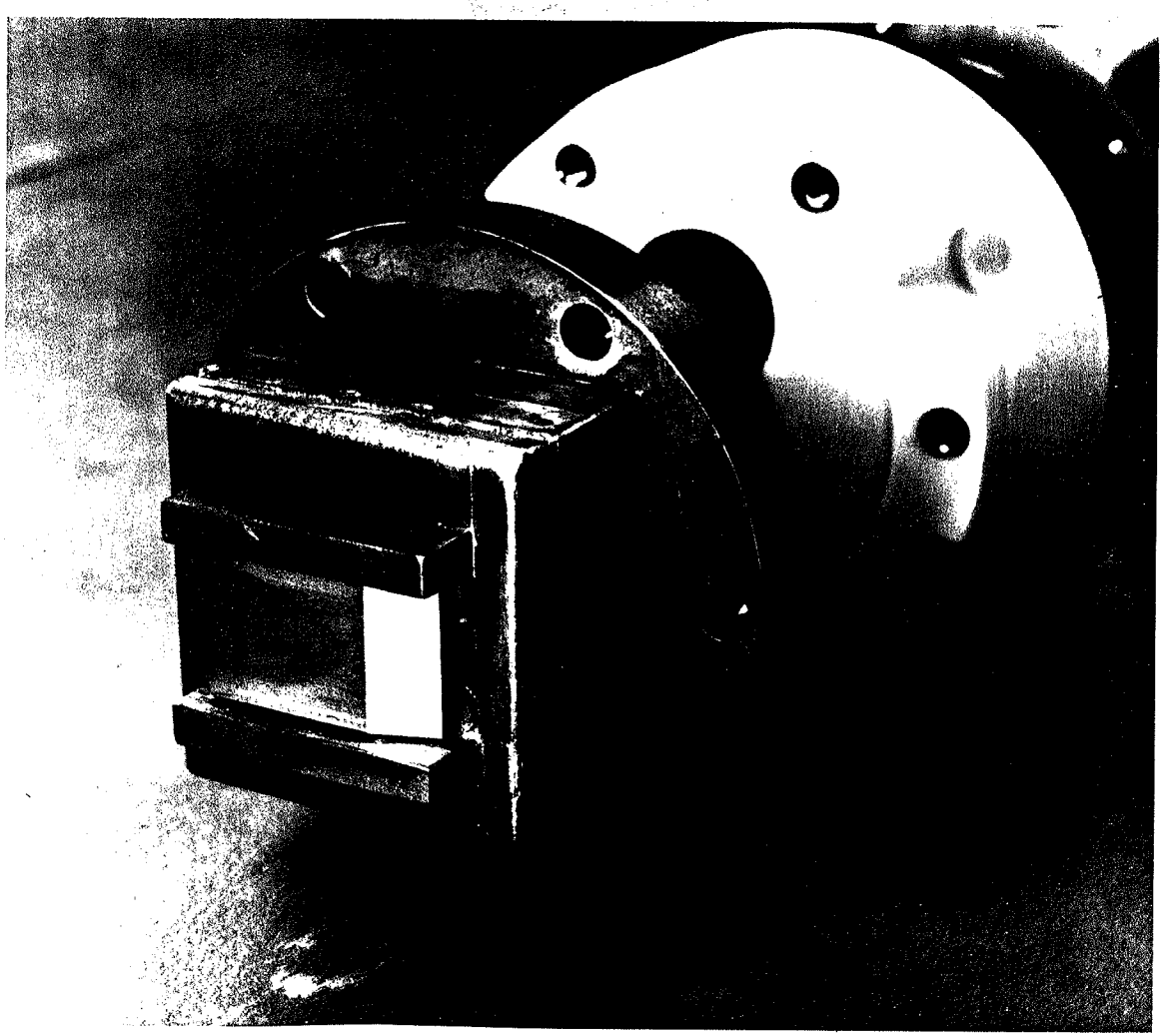

Figure 20. -- Photograph of the target assembly for the neutron therapy cyclotron. The Beryllium insert is at the left with its tapered leading edge for beam spreading, the target shaft is at the right, and the Macor target insulator is in the center.

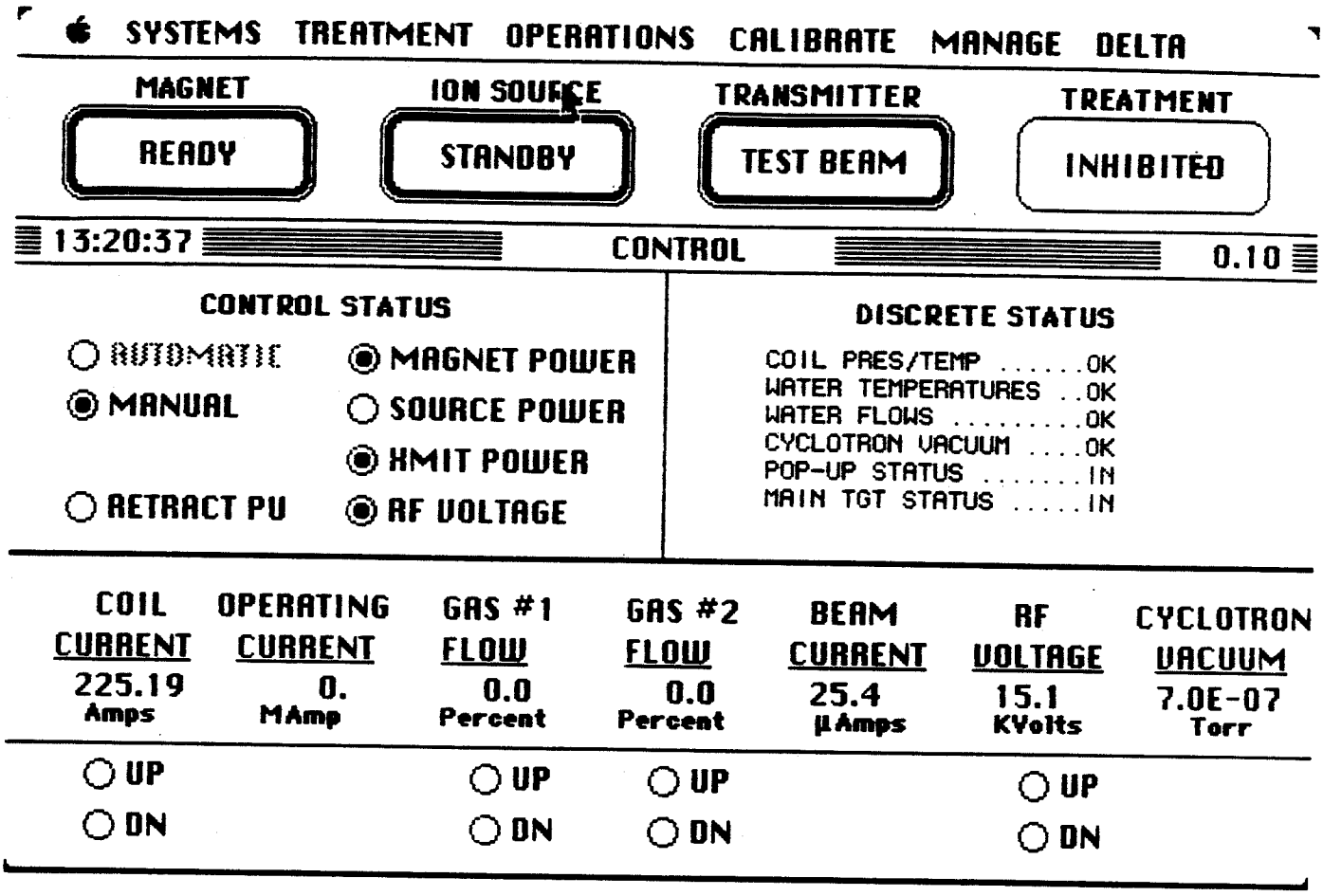

Figure 22. -- Control panel layout for normal operation of the cyclotron.

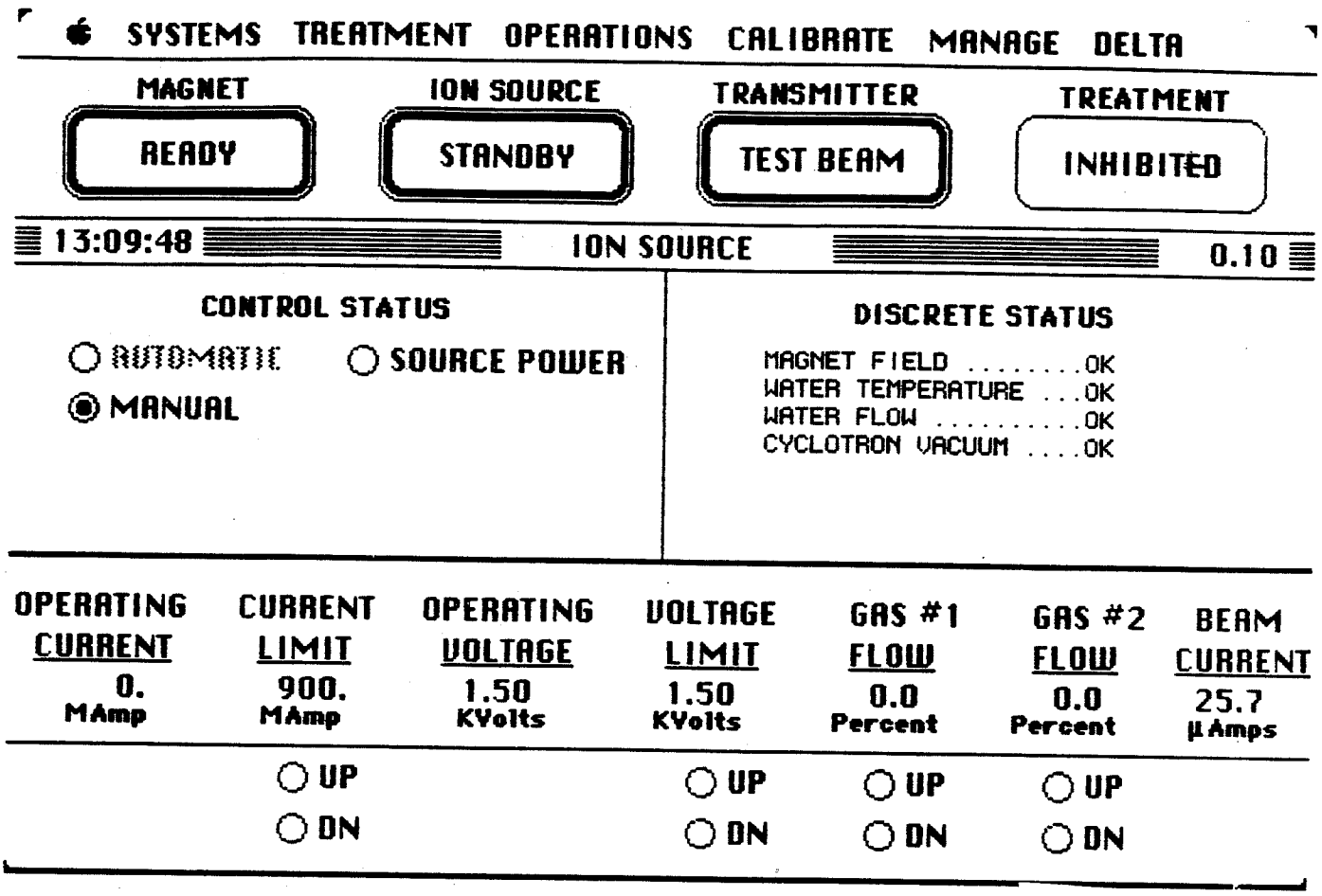

Figure 24. -- Control panel layout for specialized ion source operation.

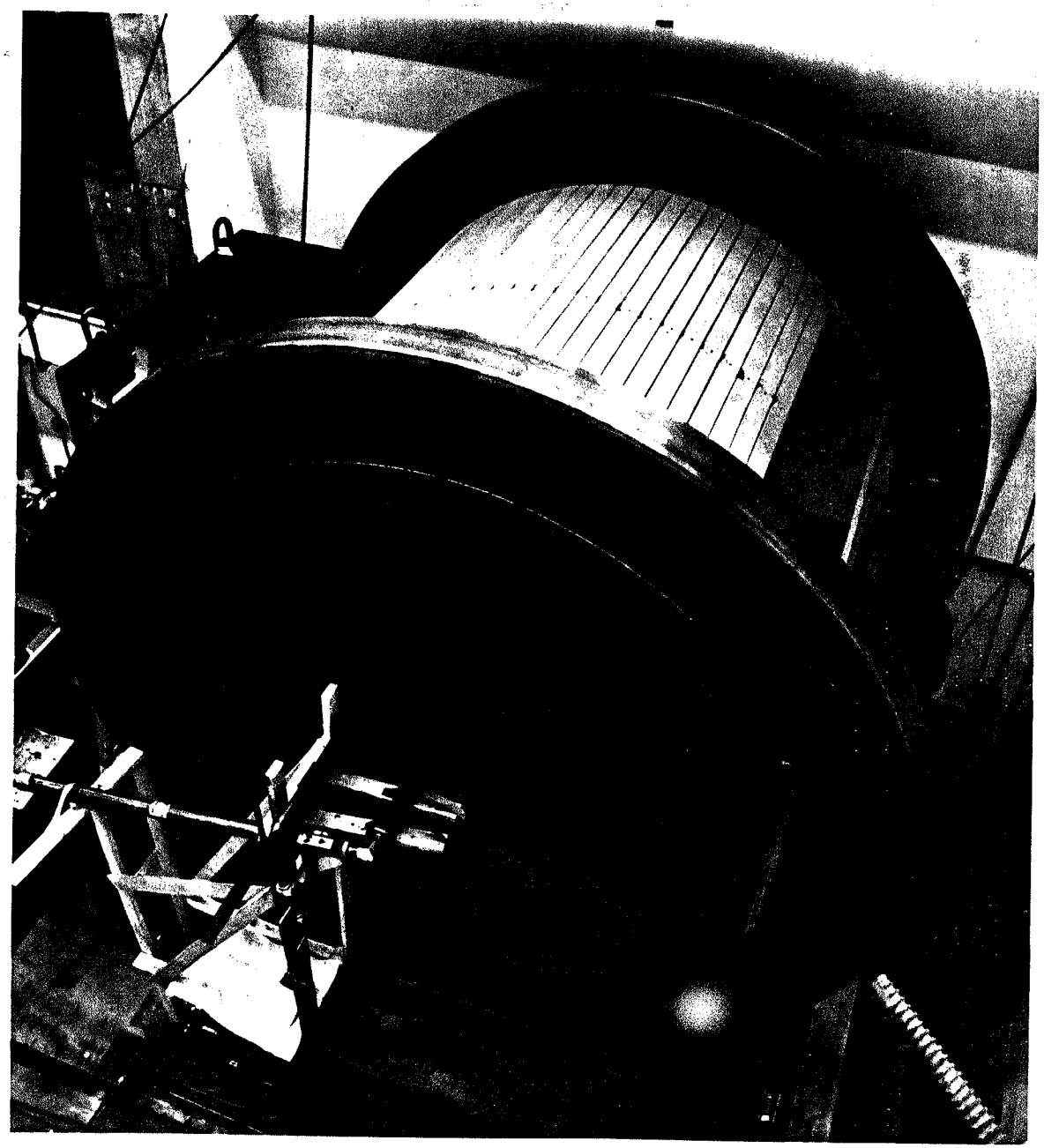

Figure 26. -- A photo of a portion of the fixed cylindrical wall separating the treatment area from the equipment area after mounting on the main gantry rings.

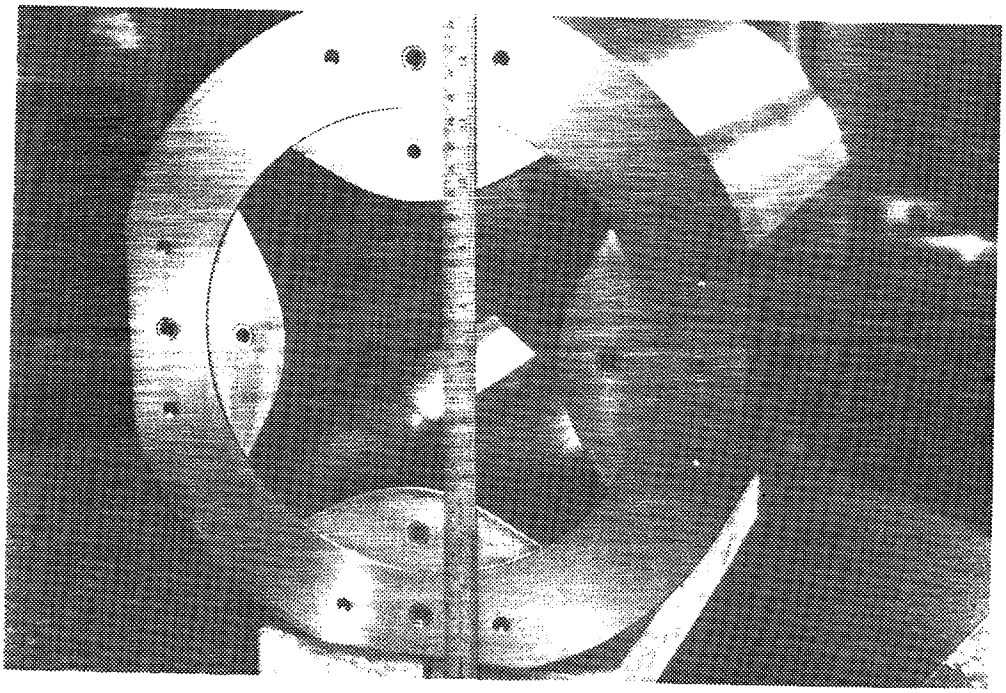

Figure 13.

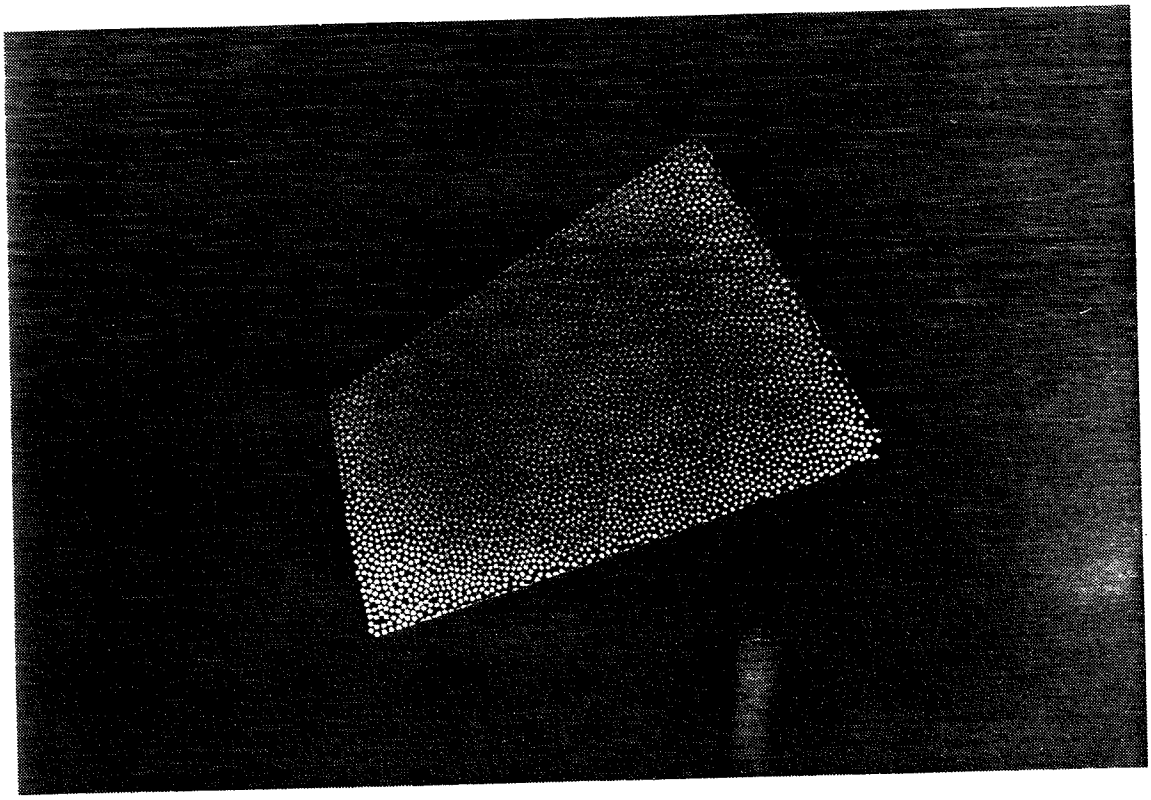

Figure 14.

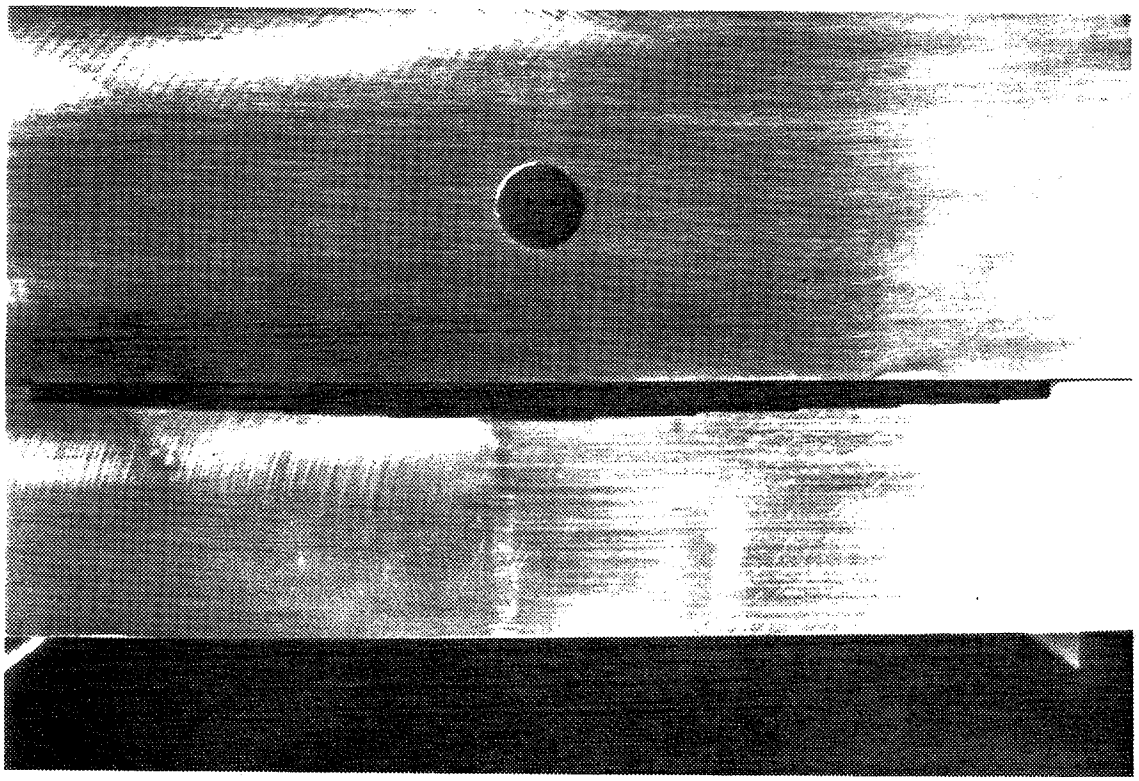

Figure 8.